ELSEVIER

Surface Science 414 (1998) 209–220

surface science

Growth modes of vanadium and iron on V(110) single crystals

T. Nawrath *, H. Fritzsche, H. Maletta

Hahn-Meitner-Institut Berlin, Glienicker Strasse 100, D-14109 Berlin, Germany

Received 2 March 1998; accepted for publication 10 June 1998

Abstract

In this paper we present investigations on the growth of the bcc structured metals vanadium and iron on V(110) single crystals in the thickness range 0–20 Å. For the analysis we used low energy electron diffraction (LEED) and Auger electron spectroscopy (AES). The growth was performed by molecular beam epitaxy (MBE) at 320 K and 570 K for vanadium and at 320 K and 470 K for iron. For both materials we observe a strong change in the growth modes from 320 K to 470 K and 570 K, respectively. For vanadium we observe well-ordered surfaces at $T=320$ K for $t_V>10$ Å with a different island size of 89 Å and 50 Å in the [001] and [1$\bar{1}$0] direction, respectively. For $T=570$ K a change of the growth mode is observed, represented by a quasi-periodic sequence of up and down staircases in the [1$\bar{1}$0] direction with inclinations of 50° with respect to the film plane and the ridges orientated along the [001] direction. For iron we find a quasi-Frank–van der Merwe growth at 320 K with an anisotropic island size for the [001] and [1$\bar{1}$0] direction, with larger values by a factor of 1.5–2.0 in the [001] direction. The island size is smaller than that for V on V(110) in the whole thickness range and we observe a minimum of island size at $t_{Fe}=4$ Å. At $T=470$ K, the growth also changes to a faceted growth mode, with the facets in the same orientation as for vanadium, but with an inclination of $\pm 40°$ with respect to the film plane.

Keywords: Auger electron spectroscopy; Epitaxy; Iron; Low energy electron diffraction (LEED); Magnetic films; Single crystal surfaces; Surface structure; Vanadium

1. Introduction

It is well known that the surface and interfaces of magnetic thin films play a fundamental role in explaining the observed behaviour of properties like magnetization, magnetic anisotropy or coupling between two magnetic films through a non-magnetic spacer layer. Furthermore, both experimental [1–5] and theoretical [6–8] contributions emphasize the importance of the surface (interface) topology to these properties. According to this, growth studies seem to be a compulsory topic preceding the study of the thin film magnetism itself. This includes the growth of the magnetic film, as well as its non-magnetic neighbour.

In this article we want to focus on the growth of iron and vanadium on V(110) single crystals. Concerning the growth of thin films, these systems are not very well studied, although it might be of interest in comparison to the very well known growth of Fe on W(110) [9–11] as both vanadium and tungsten have a larger lattice constant than iron (Fe: 2.87 Å; V: 3.02 Å; W: 3.16 Å) with the same crystalline structure (bcc) for all metals. In contrast to vanadium, W has a much higher free surface enthalpy than Fe (Fe: 2.939 J/m^2; V: 2.876 J/m^2; W: 3.468 J/m^2 [12]). According to the

* Corresponding author. Fax: +49 30 8062 2523; e-mail: nawrath@hmi.de

0039-6028/98/$ – see front matter
PII: S0039-6028(98)00513-5

arguments of Bauer and van der Merwe [13,14], the interplay between the lattice constant and the free surface enthalpy gives rise to the growth mode of the particular system. For W/Fe the larger free surface enthalpy of W can explain the pseudomorphic growth of Fe within the first two monolayers [9,10]. As the free surface enthalpy of vanadium is slightly smaller than that of Fe, it is probable that the growth differs from the W/Fe system. A closer comparison between these two systems could give some further hints on the importance of lattice mismatch to the growth modes for metallic systems.

Concerning its magnetic behaviour, the interlayer coupling of Fe in Fe/V multilayers [15–17] became an important subject of comparison to the very prominent and strongly RKKY coupled Fe/Cr multilayers [18–20].

Further on, the predicted and partly measured antiferromagnetic polarization of vanadium in the vicinity of the Fe(110) interface [21,22] (for the (100) surface see also Refs. [23,24]) is of interest for basic research programs. Here, vanadium is of particular interest as it is an ideal substrate for the newly developed field of in situ magnetization measurements of ultrathin films with polarized neutrons (in situ PNR) [25].

2. Experimental

All samples were evaporated on a vanadium (110) single crystal, which had dimensions of $30 \times 12\ mm^2$ and was orientated with an accuracy of 0.25° with respect to the surface normal. It could be heated by a graphite layer embedded in boron nitride, which was positioned behind the single crystal, up to a temperature of 1400 K. The sample temperature was measured with a chromel/alumel thermocouple, which was in direct contact with the sample holder.

To clean the V single crystal from its impurities, mainly sulphur, carbon and oxygen, repeated cycles of sputtering with a 400 eV argon beam and annealing at 1200 K were performed. To clean the surface, 2 min sputtering at a beam current of 10 μA was sufficient, as could be verified by AES. In order to recrystallize and smooth the crystal surface, the crystal must be annealed at a temperature of 1200 K for 20 min. However, this annealing process leads again to a surface contamination. Therefore, the sputter annealing cycle must be repeated for approximately 120 h to get a smooth and clean V(110) surface. Similar cleaning procedures for vanadium are also described in Refs. [26–28]. After this initial cleaning procedure of the surface, new experiments could be performed after an entire cleaning time of 12 h.

All measurements were performed under UHV conditions with a base pressure less than 10^{-10} mbar and a pressure during evaporation less than 2×10^{-10} mbar. The vanadium and iron films were prepared by an electron beam evaporator at a rate of 0.07 Å/s. All films as well as the annealed crystal were checked for surface contaminations with AES. The detection limit of this method is 2% of a monolayer for Auger transitions that have no overlap with transitions of the film or the substrate. For oxygen the main transition (KLL) at 514 eV is relatively close to that of the V-LMM transition at 509 eV. However, as the transition probability of the V-LMM peak is small, oxygen contaminations can be detected at a modulation amplitude of the Auger analyser of 2 eV due to an energy shift and an increase of the V-LMM peak. The sensitivity for oxygen contaminations is about 5%. For all experiments presented in this article, the surface contaminations were beyond the detection limit of the Auger spectroscope.

The thickness of the films was monitored by a quartz balance which had been calibrated by measurements and simulations of the X-ray reflectivity (low angle X-ray diffraction) of thicker films (e.g. V(110)/10 Å V/6 Å Fe/300 Å Cr). From these simulations, which treat the interface reflectivity as known from optics, described by the Fresnel reflectivity that is multiplied by a Debye–Waller factor for the interfacial roughness [29–31], the mean square surface roughness of the interfaces can be deduced, too. From this a typical value for the roughness of the V/Fe and Fe/Cr interfaces was 3 Å.

To perform our measurements in dependence on the thickness, the films were evaporated as wedges on the single crystal. The data presented later in Figs. 3 and 6–8 were obtained from wedges with

an inclination of 0.6 Å/mm, whereas the data of Figs. 9 and 10 were acquired from wedges with an inclination of 1 Å/mm.

For the characterization of the films, a CMA Auger electron spectroscope and a rear view LEED system were applied with a spot size of the electron beam of 100 μm and 400 μm, respectively. Therefore the data acquired from the wedges are averaged over a thickness Δt of 0.06 Å (0.1 Å) for the LEED and 0.24 Å (0.4 Å) for the AES measurements. For a quantitative analysis of the LEED patterns, a digitalizing CCD camera was used with a resolution of 512×512 pixels and a dynamic of eight bits.

All measurements were performed directly after evaporation. The total data acquisition time was about 15 min for the LEED and 1 h for the Auger measurements. During this time no change of the films could be detected.

3. Data evaluation

As mentioned above, the AES was used to prove the cleanliness of the crystal. In addition it can be applied to characterize the growth mode of a film, by studying the decrease (increase) of substrate (film) Auger transition intensities as a function of film thickness. If one assumes Frank–van der Merwe growth (layer by layer), these intensities can be described in the following way for each integer of evaporated atomic layers.

The substrate intensity is given by:

$$I_S \, e^{-t/\lambda_1 \cos\theta} \tag{1}$$

and the film intensity by:

$$I_F(1-e^{-t/\lambda_2 \cos\theta}) \tag{2}$$

where I_S and I_F are the Auger intensities of the pure substrate and film, respectively, t represents the thickness of the film, and θ the angle of emission of the Auger electrons with respect to the surface normal. A cylindrical mirror analyser (CMA) detects only electrons with $\theta = 42^\circ$. The mean free path λ_i of the Auger electrons is a function of the particular Auger energies.

For an ideal Frank–van der Merwe growth, where atoms at the $(n+1)$th layer occur only when the nth layer is completely filled, the Auger intensity at a non-integer layer thickness r, with $n < r < n+1$, is given by a linear superposition of the integer intensities, leading to kinks in an Auger intensity versus film thickness plot. However, this behaviour is not fulfilled in many systems.

As an example, where STM and AES studies show a contrasting behaviour concerning the observation of Auger kinks and Frank–van der Merwe growth, we want to discuss the growth of Fe on W(110). It is well known that Fe grows pseudomorphically on W in the first monolayer with an almost full completion of the layer, before the second layer starts to grow [11]. From the second to the third layer there is a more continuous transition, as the nucleation of the third monolayer starts when the second monolayer is not yet completely filled. From this one should expect an Auger kink after the completion of the first pseudomorphic monolayer, but not necessarily after the second one. In contrast to that the only (and very clear) Auger kink occurs at an Fe coverage which corresponds to two pseudomorphic monolayers [9,32]. Therefore two points can be concluded.

(1) Auger kinks are not a clear sign for the completion of an atomic layer. A change in the growth mode can also lead to kinks.
(2) Even if the model of a layer by layer coverage of the substrate is almost completely fulfilled, as for Fe on W(110) in the first two monolayers, this does not necessarily lead to the observation of Auger kinks.

Hence we want to speak of quasi-Frank–van der Merwe growth, if there is no observation of kinks, but the averaged increase (decrease) of the Auger intensities is comparable to that of Frank–van der Merwe growth.

In this article the different growth modes of Fe and V on V(110) were studied according to Eqs. (1) and (2). Other growth modes such as Stranski–Krastanov, Vollmer–Weber or a growth mode that leads to a faceted surface have a larger deviation of the mean film thickness. Due to the exponential decay in Eqs. (1) and (2), such a local variation of the thickness results in a smaller decrease of the substrate intensity as well as a smaller increase of the film intensity.

The Auger data were evaluated from the Auger

intensities of the Fe-$L_3M_{45}M_{45}$ (703 eV) and the V-$L_3M_{23}M_{45}$ (473 eV) transitions to characterize the growth mode. For these two electron energies the mean free paths are 14.3 Å and 11.8 Å, respectively [33].

For structural studies we also refer to the LEED measurements, as all the films presented here grew in single crystalline modes.

We also want to discuss briefly two LEED structures arising from two different types of growth. The first one is a surface with islands (or nucleation centres) of a certain size on it. This leads to an energy independent broadening of the diffraction spots, whereas the width of the spots increases with decreasing island size. The important observables are indicated in Fig. 1a, where the diffraction patterns of the clean vanadium (110) surface are shown. One can see the {10} LEED spots together with the in-plane reciprocal lattice vectors $K_{1\bar{1}} = 2\pi/d_{1\bar{1}0}$ and $K_{11} = 2\pi/d_{001}$. The length $d_{1\bar{1}0} = \sqrt{2}a/2$ and $d_{001} = a/2$ are the distances of the atomic rows in the particular lattice directions with the vanadium lattice parameter a. One can also define the full-width at half-maximum (FWHM) ΔK_{11} and $\Delta K_{1\bar{1}}$ of the LEED spots in the specific crystal directions, as also denoted in Fig. 1.

From K_{ij} and ΔK_{ij} the number of atoms per island N_{hkl} can be determined as [34]:

$$N_{1\bar{1}0} = \frac{K_{1\bar{1}}}{\Delta K_{1\bar{1}}} \tag{3a}$$

$$N_{001} = \frac{K_{11}}{\Delta K_{11}} \tag{3b}$$

The island size can easily be evaluated:

$$l_{hkl} = N_{hkl} d_{hkl} \tag{4}$$

We also want to mention that the value of $K/\Delta K$ can generally be interpreted as the number of correlated atomic rows in a particular direction, which is equivalent to the island size in the model presented here.

The other type of growth is that of a faceted surface, as indicated in Fig. 2, consisting of up and down staircases in one specific crystal direction (here the $[1\bar{1}0]$ direction with $d_{1\bar{1}0}$ as the spacing

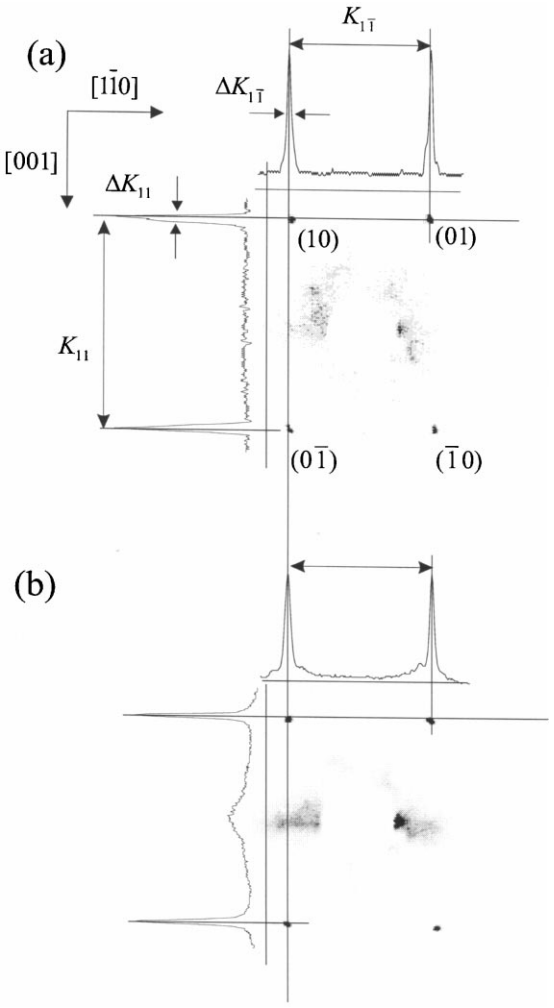

Fig. 1. LEED pattern at $E = 70$ eV of: (a) the pure V(110) crystal; (b) 10 Å vanadium evaporated on V(110) at $T = 320$ K. The orientation of the crystal relative to the pattern is indicated at the right side of the figure. The intensity profiles are drawn along the indicated lines in the LEED pattern.

of adjacent atomic rows). In this case the diffraction pattern consists of the ordinary in-phase diffraction spots together with satellites that change their reciprocal distance to the central spike proportional to $\Delta K_z = K_z - K_{z\ \text{in-phase}}$. $K_{z\ \text{in-phase}}$ represents the K_z value of the particular in-phase condition ($K_z d_z = 2\pi n$), as plotted in Fig. 2. K_z is the z-component of the scattering vector $\boldsymbol{K} = \boldsymbol{k}_f - \boldsymbol{k}_i$, with $\boldsymbol{k}_i$ and $\boldsymbol{k}_f$ as the initial and final electron wave vector, given by the electron mass

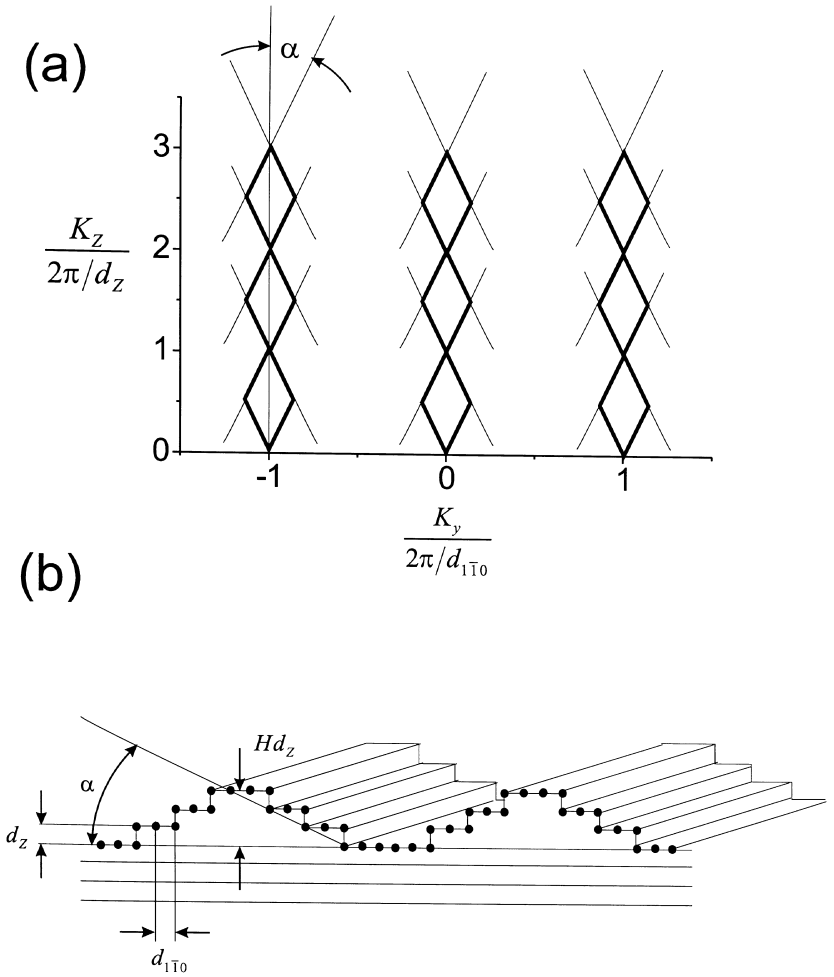

Fig. 2. (a) The reciprocal lattice of a faceted surface as sketched in (b).

m_e and the energy E as $\hbar|\boldsymbol{k}_{i,f}|=\sqrt{2m_eE}$, respectively. The angle α as indicated in the reciprocal pattern (Fig. 2) corresponds to the angle of inclination of the staircases in real space [35,36].

For a periodic structure as shown in Fig. 2, the intensity dependence of the central spike $I_0(K_z)$ can also be calculated in a kinematic model for the first atomic layer. With Hd_z as the height of the facets and each terrace at levels md_z ($m=0$, 1, …, H), the intensity I_0 is given by: $I_0/I_{00}=|\Sigma\,\theta_m\exp(ik_zmd_z)|^2$, where the factor θ_m is the portion of each terrace compared to the whole surface (with $\theta_m\cong 1/(H+1)$) and I_{00} is the intensity of the ideal flat surface. From this one obtains the well-known diffraction pattern of a grating with $(H+1)$ slits:

$$I_0(K_z)/I_{00}=\sin^2[K_zd_z(H+1)/2]/\sin^2(K_zd_z/2) \quad (5)$$

4. Results

4.1. Growth of vanadium at 320 K

We first want to present the results of vanadium grown on V(110), which is also used as a substrate for the Fe wedges presented in Sections 4.3 and 4.4. We had to rely only on our LEED measure-

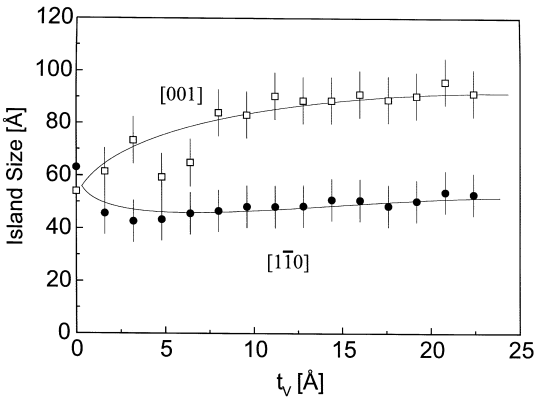

Fig. 3. Island size of vanadium prepared at 320 K on V(110) in dependence on the evaporated vanadium thickness t_V. The island size in the [1$\bar{1}$0] (solid circles) and [001] direction (open squares) is plotted.

ments as AES is not suitable for homoepitaxial growth.

Fig. 1a shows the LEED pattern of the pure vanadium crystal at an energy of 70 eV. One can see the {10} spots, as indicated in the picture. The orientation of the substrate is indicated by two arrows for the [1$\bar{1}$0] and [001] direction. The two profiles of the spots along these directions are also shown. It can be seen that ΔK is approximately the same in both crystalline directions. Fig. 1a can also be seen as proof of the absence of oxygen on the surface, as this results in a (6×2) superstructure [28].

In Fig. 1b a LEED picture of a 10 Å thick V film (no wedge sample) grown at $T=320$ K is shown, also with the profiles of the {10} spots. Here an anisotropy in ΔK can be seen, which leads to an anisotropic island size according to Eqs. (3a), (3b) and (4). From that we get the number of atomic rows N in the [001] and [1$\bar{1}$0] direction with 49.3 ± 4.9 and 23.8 ± 2.7 atomic rows, which corresponds to an island size of 74.7 ± 7.4 Å and 50.8 ± 5.7 Å, respectively.

In Fig. 3 the island size for the [001] and [1$\bar{1}$0] direction is plotted versus the thickness of the vanadium evaporated at 320 K. These data were taken from wedges as described in Section 2. One can clearly see the different behaviour for the two crystalline directions. For $t_V=0$ Å the island size is larger in the [1$\bar{1}$0] direction. That changes in the thickness range $t_V=0$–7 Å. For $t_V>10$ Å a saturation value for the island size of 89 ± 8 Å in the [001] direction and 50 ± 6 Å in the [1$\bar{1}$0] direction is observed.

4.2. Growth of vanadium at 570 K

When increasing the evaporation temperature to 570 K, the shape of the LEED patterns changes entirely. This is shown in Fig. 4, where the LEED pictures of a 50 Å thick V film on V(110) are shown with electron energies of 56, 68, and 76 eV.

At an energy of 68 eV the {10} peaks are also

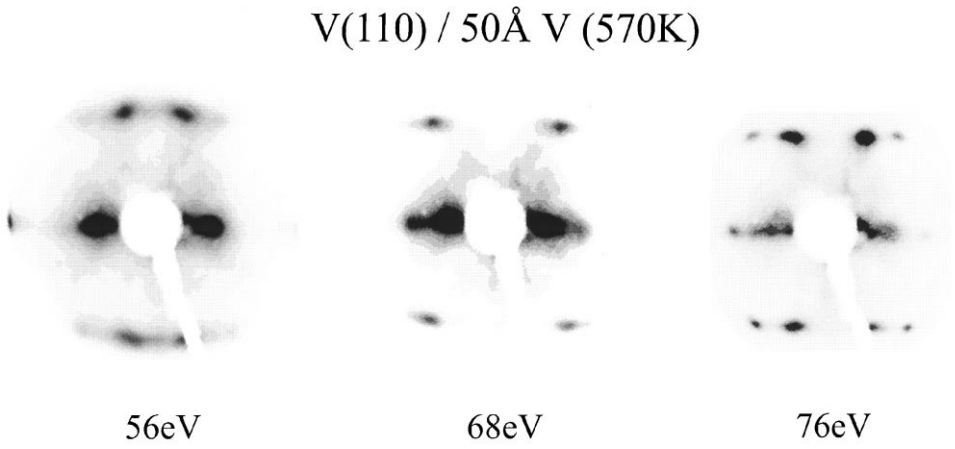

Fig. 4. LEED patterns of a 50 Å vanadium grown on V(110) at electron energies $E=56$, 68, and 76 eV. The evaporation temperature was 570 K. $E=68$ eV corresponds to the in-phase condition of the {10} spots.

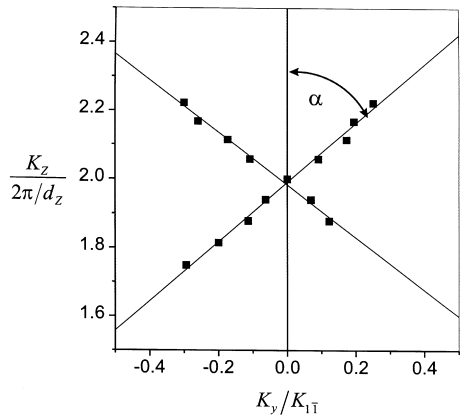

Fig. 5. Position of the {10} spot satellites in reciprocal space of 50 Å V on V(110) at 570 K. The angle $\alpha = 50 \pm 2^\circ$ corresponds to the inclination of the facets with respect to the film plane.

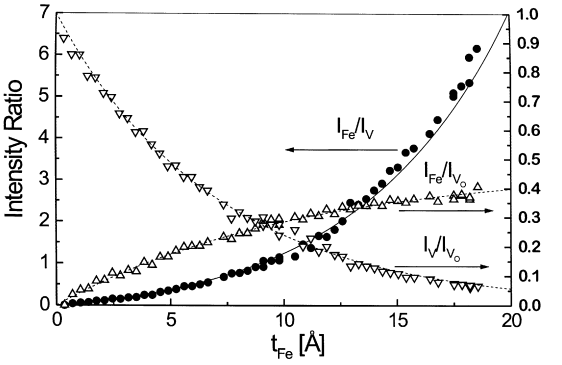

Fig. 6. The Fe and V Auger intensities of Fe prepared on V(110)/10 Å V at 320 K versus the iron thickness t_{Fe}. The lines are fits as mentioned in the text.

elliptically shaped with the longer side in the $[1\bar{1}0]$ direction. However, if the electron energy is increased up to 76 eV (Fig. 4c), one can see an energy dependent splitting of the peaks into two satellites. This behaviour is not observed for the V films grown at 320 K. The observation of such a pattern as a function of energy can be explained by a faceted surface, as discussed in Section 2. The up and down staircases are orientated along the $[1\bar{1}0]$ direction and the ridges along the [001] direction. The height of the facets Hd_z can be estimated due to the disappearance of the central spike at energies of 66 eV and 74 eV, according to Eq. (5), to 20 ± 6 Å.

In Fig. 5 the position of the {10} satellites is plotted in reciprocal space. A clear analogy to the linear dependence of the satellites in Fig. 2a can be observed. Here K_y corresponds to the $[1\bar{1}0]$ direction. A fit to the data gives an angle $\alpha = 50 \pm 2^\circ$. This is a slightly higher inclination than $\alpha = 45^\circ$, which corresponds to alternating (100) and (010) planes.

4.3. Growth of iron on V(110)/10 Å V at 320 K

Iron was grown on V(110) with a cap layer of 10 Å vanadium, also grown at 320 K. The topology of this substrate was described in Section 4.1. All experiments presented in this section are performed on wedges.

In Fig. 6 the Auger intensities of the Fe-$L_3M_{45}M_{45}$ (703 eV) edge and V-$L_3M_{23}M_{45}$ (473 eV) edge are presented. The Fe intensity I_{Fe}, represented by up triangles, shows an increase due to the increasing Fe thickness t_{Fe}, whereas the V intensity I_V (down triangles) decreases for the same reason. Both intensities are normalized to the intensity I_{V0} of the pure vanadium surface. One can see that the saturation value for the Fe peak intensity is smaller than that of the V peak of the uncovered surface (47% in the fit). This is due to the smaller transition probability for the pure iron peak compared to that of vanadium ($I_{Fe}/I_V = 0.52$ [37]). Also shown is the intensity ratio (Fe-LMM intensity/V-LMM intensity), which has a strong uprise because of the increasing (decreasing) intensities of Fe (V), respectively. The data are fitted (straight lines) due to Eqs. (1) and (2), assuming an electron mean free path of 13.4 ± 1.3 Å for the 703 eV iron Auger electrons and 9.4 ± 1.3 Å for the 473 eV vanadium Auger electrons.

The LEED patterns for this growth temperature are presented in Fig. 7 for Fe thicknesses of 6.2 Å, 10 Å, and 16.5 Å. The cross-sections of the spots in the $[1\bar{1}0]$ and [001] directions are also plotted. It can be seen that ΔK at $t_{Fe} = 10$ Å and 16.5 Å is larger in the $[1\bar{1}0]$ direction. This indicates a larger average island size in the [001] than in the $[1\bar{1}0]$ direction, as for V on V(110).

In Fig. 8a this island size is plotted versus the Fe thickness for the [001] direction (down triangles) and for the $[1\bar{1}0]$ direction (up triangles). It

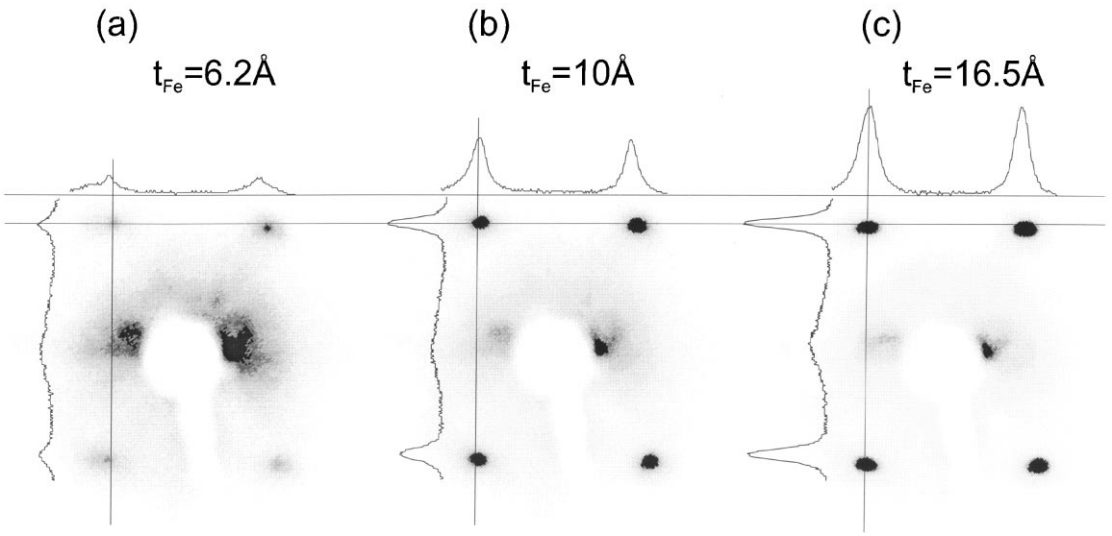

Fig. 7. LEED patterns at 70 eV of Fe on V(110)/10 Å V prepared at a growth temperature of 320 K. The spot profiles are also shown.

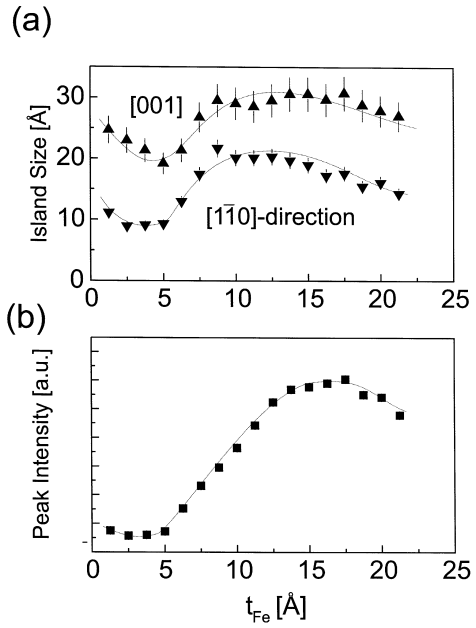

Fig. 8. Fe on V(110)/10 Å V at an evaporation temperature of 320 K. (a) Island size in the [1$\bar{1}$0] and [001] directions in dependence on the Fe thickness t_{Fe}, in (b) the peak intensity of the {10} spots at 70 eV is plotted versus t_{Fe}.

can be seen that in both crystalline directions the island size decreases in the range from 0 to 3 Å Fe thickness, reaching a minimum at about $t_{Fe}=4$ Å. This collapse to values of 21 ± 2 Å and 9 ± 1 Å for the [001] and [1$\bar{1}$0] directions is much smaller than the island size of the vanadium surface, which has typical values of 89 Å (50 Å) along [001] ([1$\bar{1}$0]) for 10 Å V on V(110). In the range 6–8 Å the Fe surface gets more ordered again in both directions, reaching a maximum value at $t_{Fe}=12$ Å. For higher t_{Fe} values there is a slow decrease in the island size visible.

It is remarkable that, despite the different island sizes in the main crystalline directions, their characteristic behaviour with respect to t_{Fe} remains the same in the whole thickness range, i.e. a factor of 1.5–2.0 bigger terrace width in the [001] than in the [1$\bar{1}$0] direction.

In Fig. 8b the peak intensities of the {10} spots at an energy of 70 eV are plotted versus t_{Fe}. The intensity also rises in the range of 6–8 Å, with a maximum at about 15 Å. In accordance with the island size the peak intensity also decreases above 17 Å.

4.4. Growth of iron at 470 K on V(110)/10 Å V (320 K)

For the investigations on the growth of Fe on V, a lower temperature was chosen to avoid an intermixing of Fe and V in the low thickness range

due to diffusion. Again, all experiments described in this section were performed on wedge samples.

The LEED patterns of iron on V(110)/10 Å vanadium grown at 470 K are very similar to those of vanadium on V(110) at 570 K. One can see a splitting of the LEED spots in the [1$\bar{1}$0] direction in dependence on the electron energy, indicating facets with the same orientation as for the V films grown at 570 K.

In Fig. 9 the splitting of the {10} spots for a 30 Å thick Fe film on V(110) is illustrated, where the position of the satellites is plotted in reciprocal space. As the angle α is $40\pm2^{\circ}$, one does not get exactly repeated (001) and (010) surfaces in the [1$\bar{1}$0] direction. Here the height Hd_z of the facets can be estimated as 22 ± 6 Å in the same way as described in Section 4.2.

The Auger intensities of the V- and Fe-LMM peaks show a different behaviour compared to the growth at 320 K (Fig. 10). The increase (decrease) of the Fe-$L_3M_{45}M_{45}$ (V-$L_3M_{23}M_{45}$) peak as a function of t_{Fe} is slower than for the growth at 320 K. As a consequence, the ratio of Fe-$L_3M_{45}M_{45}$ to V-$L_3M_{23}M_{45}$ also has a much smaller increase (the lines are guides to the eye).

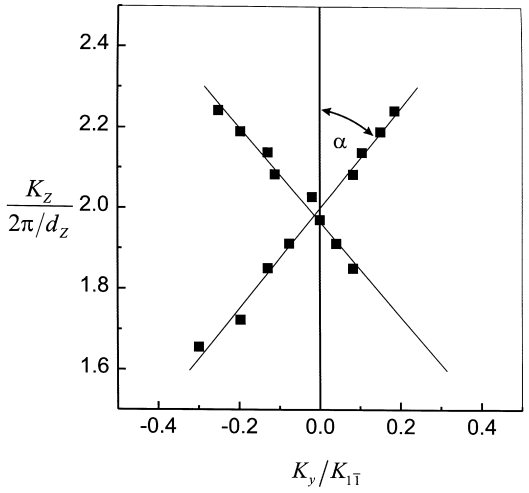

Fig. 9. Reciprocal position of the {10} spot satellites of a 30 Å thick Fe film grown at 470 K on V(110)/10 Å V. The angle $\alpha=40\pm2^{\circ}$ corresponds to the inclination of the facets with respect to the film plane.

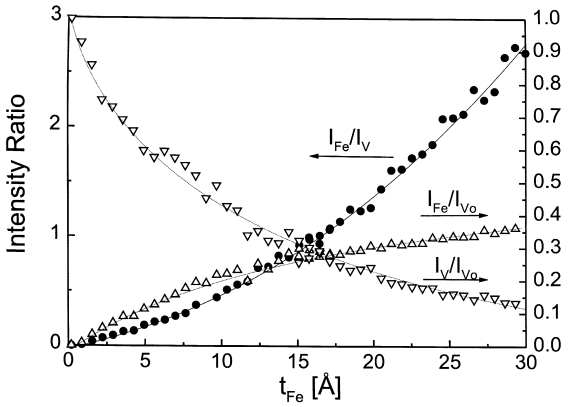

Fig. 10. Dependence of the Auger intensities of Fe and V on t_{Fe} at an evaporation temperature of 470 K. The lines are guides to the eye.

This indicates a larger deviation from the averaged iron thickness for the growth at 470 K compared to the growth at 320 K.

5. Discussion

First we want to discuss the growth on V(110) at 320 K. There is a similar behaviour of the Fe and V films concerning the anisotropic island size, as for both systems the island size is much bigger in the [001] direction than in the [1$\bar{1}$0] direction. This can be seen impressively for the growth of vanadium on V where the system starts at an island size of 55 ± 5 Å and 63 ± 6 Å for the [001] and [1$\bar{1}$0] direction, respectively. Above $t_V=10$ Å the system reaches its saturation values of 89 ± 8 Å and 50 ± 6 Å in the different crystalline directions. The island sizes which were obtained from a V film with $t_V=10$ Å are in accordance with the data of the wedge sample within the error limits. The ratio between the island size in the [1$\bar{1}$0] and [001] direction is approximately the same for the V/V (1.8) and the V/Fe system (1.5–2.0).

A point of consideration is whether the anisotropy of the 10 Å V surface predetermines the observed anisotropy of the Fe islands. Keeping in mind that the island size of the substrate is about four times larger in both directions in the thickness range up to $t_{Fe}=5$ Å, an influence of the substrate

structure on the film structure can be excluded. For larger Fe thickness the island size of the film increases, but due to the Auger data the V surface is completely covered, so that there is no interaction between the Fe atoms on the surface and the V edges.

The collapse of the Fe island size is only observed for the V(110)/Fe system and not for the V(110)/V system. That underlines the special behaviour of the Fe epitaxy on V. A reason for this behaviour could be a hindered island coalescence due to the lattice mismatch of V and Fe, as also discussed for Fe on W(110) [11,38]. The result of this mismatch is that an Fe island that is more or less pseudomorphic will always have a partly relaxed lattice at the edges, where the Fe atoms are shifted towards the centre. For further Fe atoms the profit in energy will therefore decrease with increasing island size, as the misfit of the outer Fe atoms increases. This can lead to a situation where the formation of many small islands is energetically more advantageous than the formation of a few big ones. As the free surface enthalpy of vanadium is small, this formation could occur at a relatively small island size, which causes this rather uncorrelated structure up to $t_{Fe}=5$ Å.

In order to decide whether there is pseudomorphic growth in this thickness range, a direct measurement of the Fe lattice constant had to be performed, which is not feasible as the FWHM of the LEED spots is too big to give a precise value for the lattice constant. Here a limit for diffraction methods is reached, which could only be overcome by real space studies, as e.g. STM (scanning tunnel microscopy).

In this context we want to discuss an alternative growth model, which also occurs in some cases, when the evaporated film has to equalize the lattice mismatch of the substrate. This growth has been observed e.g. for Fe on W(110) [9,11], where the lattice mismatch results in periodic lattice distortions which is characterized by a Vernier period

$$p=\frac{ab}{a-b} \tag{6}$$

with a and b the lattice constants of the substrate and the film, respectively. In the LEED patterns this results in satellites around the {10} spots that have an energy independent reciprocal distance of $g_{1\bar{1}}=K_{1\bar{1}}(b/p)$ parallel to the $[1\bar{1}0]$ direction and $g_{11}=K_{11}(b/p)$ for the [001] direction. For Fe on V one gets $p/b=20.1$, from which it can be concluded that the resolution of the CCD camera is not the limiting factor for the observation of these satellites. To observe this superstructure, which looks similar to a broad diffraction pattern of a (110) surface, a further condition for the FWHM of the {10} spots has to be fulfilled, i.e. the relative width of the spots has to be smaller than the relative distance b/p of the satellites:

$$\frac{\Delta K}{K}<\frac{b}{p} \tag{7}$$

This condition is clearly fulfilled for the V(110)/10 Å substrate in the [001] direction, but only scarcely along the $[1\bar{1}0]$ direction. Assuming periodic lattice distortions for Fe on V in the thickness range up to 5 Å, the satellites should be observable at least as lines parallel to the $[1\bar{1}0]$ direction. Further on, the observed spots for Fe on V(110) are broader in the $[1\bar{1}0]$ direction for the whole thickness range. In contradiction to this, even a satellite pattern that is smeared out in both directions would lead to rhomboid shaped {10} spots that are broader by a factor of $\sqrt{2}$ in the [001] direction. From this we exclude a growth with periodic lattice distortions.

The {10} peak intensity in Fig. 8b shows a parallel behaviour to the island size for higher values in t_{Fe} (Fig. 8a). This can be explained by the FWHM of the LEED peaks being inversely proportional to the island size and the peak intensity multiplied by the FWHM of the peaks being proportional to the number of coherent scattering atoms. Therefore the peak intensity increases in proportion to the island size, when the layer is thick enough so that the number of scattering atoms remains unchanged with increasing layer thickness.

There can be two reasons for the low intensity of the {10} spots at smaller Fe thicknesses. First

there is the small island size as discussed above; a second reason may be a change in the scattering phase between Fe and V.

From AES we get information about the coverage of the V(110) surface. From the fits to the data we get a mean free path of 13.7 ± 1.3 Å for the Fe-$L_3M_{45}M_{45}$ and 9.4 ± 1.3 Å for the V-$L_3M_{23}M_{45}$ transition. The fitted ratio of the saturated Fe intensity to the intensity of the pure vanadium surface is 0.47, which is in good agreement with the literature data [37]. The fitted mean free path for the Fe and V transitions is slightly smaller compared with the empirical curve of Seah and Dench [33], which was derived from different elements and a significantly dispersed set of data points. One can also try to compare these data with the AES measurements of other systems, e.g. the W/Fe system [9]. Here the experimental mean free path is about 3.9 Å (for the Fe low energy Auger transition at 47 eV in a fit up to the first four monolayers), which is smaller by a factor of 1.1 than the value of the empirical curve introduced in Ref. [33]. For our system the averaged factor is 1.15. From that we can conclude a coverage of the substrate similar to Fe on W(110) in the first four monolayers. Therefore this growth can be called quasi-Frank–van der Merwe in the sense discussed above. Here the missing Auger kinks can be explained by the rather disturbed ordering for $t_{Fe} < 5$ Å, as observed in the LEED patterns.

We want to mention that this special growth for $t_{Fe} < 5$ Å could also be an explanation for the absence of ferromagnetism for 6 Å Fe films on V(110) at 80 K, observed with polarized neutron reflectometry [22,25], if one assumes that the films are still paramagnetic in this thickness range.

For the growth at $T = 470$ K (570 K), both systems show faceted surfaces with the ridges along the [001] direction and the staircases in the $[1\bar{1}0]$ direction. For both systems a tendency to build {100} surfaces is clearly visible, as also reported for Fe/Cr multilayers [2]. For vanadium the angle of the staircases is $50 \pm 2^\circ$, for iron it is $40 \pm 2^\circ$. This faceting can be explained in a model with an anisotropic sticking probability of atoms at steps, being high on steps with the edges along $[1\bar{1}0]$ and low on steps along [001] [35]. It seems to be a general phenomenon of (110) orientated metallic bcc surfaces. It has also been observed for W on W [39], Fe on W [35], Fe on Cr [3,36], and Cr on W [40]. To our knowledge it is observed for vanadium and iron on V(110) for the first time.

A comparison of the Auger data taken at 320 K and 470 K shows that there must exist regions with a smaller iron thickness as the averaged thickness. This is in accordance with the faceting of the iron surface.

This special faceted topology for the iron and vanadium films grown at 470 K (570 K) could also hint at an explanation for the results of Tomaz et al. [21], where the total magnetic polarization of V and the total reduction of the Fe magnetic moment is measured for V/Fe(110) and V/Fe(100) multilayers grown at ≈ 500 K. Here the magnetic moments are identical for both orientations. If one assumes faceted V/Fe interfaces for the (110) surface, the surprisingly high V polarization per atom for this orientation could be explained. However, in a naive model, a perfect faceting of the (110) surface should give a larger total reduction of the total magnetic moment by a factor of $\sqrt{2}$ than that of a flat (100) surface, as the interface surface increases by the same factor.

As a conclusion, the crucial point was the presentation of the V(110)/Fe and V(110)/V epitaxy at different temperatures. We observed a faceting of the surface at higher and a formation of anisotropic islands at lower temperatures. There is a tendency to an unordered growth for Fe on V at 320 K, followed by a more ordered surface in the regime up to 17 Å. For larger Fe thickness the surface becomes rougher again. This behaviour cannot be seen for V on V, where a saturation value in the island size is observed in the studied thickness regime.

Acknowledgements

This work was supported by the Verbundforschung of BMFT through Grant No. 03-MA4 HMI-1.

References

[1] M. Albrecht, U. Gradmann, T. Furubayashi, W.A. Harrison, Europhys. Lett. 20 (1992) 65.
[2] W. Folkerts, F. Hakkens, J. Appl. Phys. 73 (1993) 3922.
[3] R. Coehoorn, J. Magn. Magn. Mater. 151 (1995) 341.
[4] J. Schwabenhausen, T. Dürkop, H.J. Elmers, Phys. Rev. B 55 (1997) 15119.
[5] S. Miethaner, G. Bayreuther, J. Magn. Magn. Mater. 148 (1995) 42.
[6] D. Stoeffler, F. Gautier, J. Magn. Magn. Mater. 147 (1995) 260.
[7] A. Vega, C. Demangeat, H. Dreyssé, A. Chouairi, Phys. Rev. B 51 (1995) 11546.
[8] M.E. Elzain, D.E. Ellis, J. Magn. Magn. Mater. 65 (1987) 128.
[9] U. Gradmann, G. Waller, Surf. Sci. 116 (1982) 539.
[10] M. Przybylski, I. Kaufmann, U. Gradmann, Phys. Rev. B 40 (1989) 8631.
[11] H. Bethge, D. Heuer, Ch. Jensen, K. Reshöft, U. Köhler, Surf. Sci. 331–333 (1995) 878.
[12] L.Z. Mezey, J. Giber, Jpn. J. Appl. Phys. 21 (1982) 1569.
[13] E. Bauer, Z. Kristallogr. 110 (1958) 372.
[14] E. Bauer, J.H. van der Merwe, Phys. Rev. B 33 (1986) 3657.
[15] P. Isberg, P. Grandberg, E.B. Svedberg, B. Hjörvarsson, R. Wäppling, P. Nordblad, submitted to Phys. Rev. B.
[16] P. Poulopoulos, P. Isberg, W. Platow, W. Wisny, M. Farle, B. Hjörvarsson, K. Baberschke, J. Magn. Magn. Mater. 170 (1997) 57.
[17] A. Vega, A. Rubio, L.C. Balbas, J. Dorantes-Davila, S. Bouarab, C. Demangeat, A. Mokrani, H. Dreyssé, J. Appl. Phys. 69 (1991) 4544.
[18] M.N. Baibich, J.M. Broto, A. Fert, F. Nguyen Van Dau, F. Petroff, P. Etienne, G. Creuzet, A. Friedrich, J. Chazelas, Phys. Rev. Lett. 61 (1988) 2472.
[19] J. Unguris, R.J. Celotta, D.T. Pierce, Phys. Rev. Lett. 69 (1992) 1125.
[20] M. van Schilfgaarde, F. Herman, S.S.P. Parkin, J. Kudrnovsky, Phys. Rev. Lett. 74 (1995) 4063.
[21] M.A. Tomaz, W.J. Antel, Jr., W.L. O'Brien, G.R. Harp, J. Phys.: Condens. Matter 9 (1997) L179.
[22] H. Fritzsche, T. Nawrath, H. Maletta, H. Lauter, Physica B 241–243 (1998) 707.
[23] T.G. Walker, H. Hopster, Phys. Rev. B 49 (1994) 7687.
[24] P. Fuchs, K. Todtland, M. Landolt, Phys. Rev. B 53 (1996) 9123.
[25] T. Nawrath, H. Fritzsche, F. Klose, J. Nowikow, C. Polaczyk, H. Maletta, Physica B 234–236 (1997) 505.
[26] C.M. Kim, B.D. deVries, B. Frühberger, J.G. Chen, Surf. Sci. 327 (1995) 81.
[27] T. Valla, P. Pervan, M. Milun, Surf. Sci. 307–309 (1994) 843.
[28] D.L. Adams, H.B. Nielsen, Surf. Sci. 107 (1981) 305.
[29] L.G. Parratt, Phys. Rev. 95 (1954) 359.
[30] G.P. Felcher, R.O. Hilleke, R.K. Crawford, J. Haumann, R. Kleb, G. Ostrowski, Rev. Sci. Instrum. 58 (1987) 609.
[31] V.O. de Haan, G.G. Drijkoningen, Physica B 198 (1994) 24.
[32] H.J. Elmers, Ph.D. Thesis, Technische Universität Clausthal, 1989, p. 14.
[33] M.P. Seah, W.A. Dench, Surf. Interface Anal. 1 (1979) 2.
[34] M. Henzler, Surf. Sci. 132 (1983) 82.
[35] M. Albrecht, H. Fritzsche, U. Gradmann, Surf. Sci. 294 (1993) 1.
[36] H. Fritzsche, U. Gradmann, Mater. Res. Soc. Symp. Proc. 312 (1993) 321.
[37] L.E. Davies, N.C. MacDonald, P.W. Palmberg, G.E. Riach, R.E. Weber, Handbook of Auger Electron Spectroscopy, Physical Electronics Division, Perkin-Elmer Corporation, MN, 1976.
[38] H.J. Elmers, J. Hauschild, H. Höche, U. Gradmann, H. Bethge, D. Heuer, U. Köhler, Phys. Rev. Lett. 73 (1994) 898.
[39] P. Hahn, J. Clabes, M. Henzler, J. Appl. Phys. 51 (1980) 2079.
[40] H. Fritzsche, Ph.D. Thesis, Technische Universität Clausthal, 1995.